Deep Learning Based Large-scale Histological Tau Protein Mapping for Neuroimaging Biomarker Validation in Alzheimer's Disease

Maryana Alegro[1,2,3], Yuheng Chen[1], Dulce Ovando[1], Helmut Heinsen[6,7], Rana Eser[1], Duygu Tosun[4,5], Lea T. Grinberg[1,7]

[1]Department of Neurology, University of California San Francisco, San Francisco, CA, USA
[2]Berkeley Institute for Data Science, University of California Berkeley, CA, USA
[3]Bakar Institute for Computational Health Sciences, University of California San Francisco, CA, USA
[4]Department of Radiology, University of California San Francisco, San Francisco, CA, USA
[5]Veterans Affairs San Francisco, CA, USA
[6]Julius-Maximilians University Würzburg, Würzburg, Germany
[7]University of Sao Paulo Medical School, Sao Paulo, Brazil

Correspondence: maryana.alegro@ucsf.edu

Abstract
Deposits of abnormal Tau inclusions in the brain are a well-known Alzheimer's disease (AD) pathological feature and are the best predictor for neuronal loss and clinical decline. As such, Tau is a potential in-vivo imaging biomarker that could leverage earlier AD diagnosis. In fact, there are several research initiatives to develop PET tracers for imaging Tau in the human brain. Validation of such studies, however, is only reliably performed using histological data, where Tau inclusion can be accurately located. Manually locating and segmenting Tau in such images is unfeasible since a whole human brain slice, at adequate resolution, spans several Gigabytes of data and carries thousands of inclusions. In this study we present our preliminary results on using convolutional neural networks (CNN) to automatically locate and segment Tau in whole human brain histological slides. CNNs are multi-layered representation-learning methods capable of automatically discover unknown patterns that best characterize a raw data set. Moreover, they model data in a bottom-up approach, where data is characterized by small low-level features, such as edges and connected objects, in lower layers and increases in abstraction and complexity in the following layers. Our dataset is composed of histological slices stained for AT100, AT8. Each slide was imaged in our in-house built slide scanner at 1.22μm resolution. Each image is about 82000x37000 pixel wide. On average, a whole human brain dataset has 16Tb of data. Images were preprocessed and stitched using the UCSF Wynton cluster. A UNet variant was used for Tau localization and segmentation on the full-resolution images, which was performed using a NVIDIA Titan X 12Gb GPU. We then computed Tau 'heatmaps' based on the segmented images that, in turn, were registered to the MRI.

Keywords
Machine learning, deep learning, Alzheimer's disease, histopathology, digital pathology, big data, imaging

Introduction

Alzheimer's disease (AD) is a devastating neurodegenerative disease marked by progressive loss of cognitive function as well as depression, sleep disturbances, and other neuropsychiatric symptoms. In the last decade, Alzheimer's disease was the only leading cause of death to have increased in frequency – nearly a 90% increase between 2000 and 2014. Currently, more than 5 million people over the age of 65 in the US alone have a clinical diagnosis of Alzheimer's disease, accounting for an estimated 60% to 80% of dementia cases. The cost to the US economy is well over $214 billion/year and is projected to reach $1.2 trillion by 2050 [1]. It imposes an enormous burden on society. Despite intensive research on AD neurobiology and advances in imaging technology, effective disease-modifying treatments remain elusive. It is undisputed that AD treatment is likely to be more effective if started during its asymptomatic phase. Thus, it is essential to have reliable and accurate biomarkers available to enhance detection of AD in its earliest stages, test the effectiveness of new therapies, and monitor disease progression.
Alzheimer's disease is characterized by a long silent period that can last more than a decade before symptoms onset [2]. It begins by affecting brain structures not classically associated with it, such as cortical and neocortical regions, but rather centered in the brainstem nuclei, like the Locus Coeruleus (LC) and Dorsal Raphe nucleus (DRN) [3, 4]. These regions experience progressive degeneration correlated with AD severity [5-8], including cell loss and white matter degradation [9-11]. As the disease progresses, the transentorhinal region of the brain begin to be affected[12], followed by the compromise of limbic regions such as the hippocampus. Patients begin to experience the initial symptoms, like moderate memory loss, in this stage. During the final stages, the disease extensively affects the neocortex and patients experience more severe symptoms.
AD main neuropathological hallmarks are [13]: extracellular accumulation of β-amyloid in the form of neuritic plaques [14], and intracellular accumulation of misfolded tau protein (AD-tau) – in the form of neurofibrillary tangles (NFTs), neuropil threads and dystrophic neurites [15, 16]. Its progression follows a characteristic, non-random anatomical, neuropathologically-confirmed pattern [17], on which current staging schemes are based. The amount and spreading of tau tangles directly correlate with patients' clinical decline, making it a potential biomarker for early stage AD detection.
Molecular neuroimaging techniques, such as PET scan, are the modalities with the best potential for imaging in-vivo tau tangles. In fact, researchers are investigating the development of PET tau tracer that could be used for early AD detection [18, 19]. Such tool would be ideal biomarkers to diagnose and monitor disease progression in vivo and to enable effective interventions at asymptomatic AD stages. Translation of in vivo neuroimaging features to "imaging biomarkers", however, requires extensive validation of their signal against the underlying true pathophysiology.
Voxel-to-voxel correlations between histological and neuroimaging datasets are the gold-standard approach for providing real data-driven, rather than modeling-driven, anatomical priors for validating neuroimaging modalities. Nevertheless, neuroimaging-autopsy validation studies have been limited both in number and extend, largely due to technical challenges including dataset size, computational capability and registration hurdles caused by the huge geometric differences and between neuroimaging and histology image sets.
In this study, we developed an interactive computational and histological pipeline aiming at tackling the problem of histological validation of neuroimaging modalities for tau detection. Our pipeline uses a wide range of computer vision techniques together with modern deep learning algorithms and high-performance computing (HPC) capabilities, being able to process large-scale whole human brain histological datasets, leveraging a point-to-point correlation to neuroimaging modalities. In the following sections, we provide a detailed description of the methods and quality control steps of this pipeline and the software we created. We will illustrate the utility of our pipeline for providing robust anatomical priors for validating neuroimaging methods in AD by showing unprecedented quantitative 3D whole human brain maps of tau protein detected by different antibodies at early stages.

Results

Computational Pipeline for mapping tau tangles

As a result of our research, we engineered a comprehensive computational pipeline (Figure 1) for locating and measuring the density of tau tangles in large-scale whole human brain digital pathology datasets. Our pipeline is comprised of independent modules (Figure 1, 1-6) that can be executed in parallel and are responsible for processing the different image modalities involved in the project. In the *imaging module* (Figure 1.1), we scanned our histological sections using a custom-built whole slide scanner, and stitched the raw tiles using a specialized software. Scanning time and amount of generated data was dependent of the size of the selected region of interest (ROI). On average, scanning a whole brain section took 1.5 hours, yielding approximately 1.5 thousand tiles (20Gbs of data). The stitching step took, on average, 2 days to complete on an HPC system, and generated a high-resolution histological image of approximately 80000x50000 pixels (~20Gbs). Figure 2a show an example of stitched image. The stitching step also generated a downsampled - 10% resolution version of the histological image. The blockface images created during block sectioning (see Histological processing, in Methods) were preprocessed in the *blockface preprocessing module* (Figure 1.2). First, each blockface image background was automatically removed, leaving just the brain areas. Next, all images were sorted and grouped together. Since the block or camera may have moved during sectioning, slices were manually aligned in relation to the middle slice using affine registration. Finally, slices were stacked together using in-house built software to form a 3d image volume, which was in turn used in the low-resolution histology pre-processing module.

In the *low-resolution histology pre-processing module* (Figure 1.3), the 10% resolution histological images had their background automatically segmented leaving just the brain area. White matter (WM) masks were manually created and subtracted from brain mask to create gray matter (GM) masks. The segmented low-resolution histological images were aligned to their respective pre-processed blockface images using a combination of registration algorithms and registration maps were stored for later use.

The core of our pipeline is the *high-resolution histology segmentation* module (Figure 1.4), responsible for locating the tau tangles and generating the tau density maps, here denominated heatmaps. In the heart of this module lies a convolutional neural network (CNN) responsible for segmenting the tau tangle (see Methods for a detailed description). First, datasets for CNN training were created by sampling patches of GM, extracted from random locations distributed throughout the entire 3d brain volume. A different dataset was created for AT8 and AT100 markers. These patches were randomly split into training, testing and validation datasets, yielding a total of 6 datasets. All patches were manually labeled with the help of a supervised learning segmentation algorithm. The CNN was trained using a validation data held-out scheme. High-resolution histological images were tiled into smaller images (Figure 1.4d). During this step, the low-resolution GM masks were upsampled to match the histological image resolution and, were, in turn, also tiled. Histology tiles had their background segmented using their respective mask tiles, leaving just the GM regions. This allowed us to disregard tiles that did not contain GM thus, avoiding unnecessary computations. Each tile was segmented using our trained CNN model, resulting in a probability map that was thresholded to create a binary mask. Heatmaps were computed for each tile (Figure 1.4f) and combined together to form a high-resolution heatmap (Figure 1.4g) that had the same dimension of the original histology. A 10% resolution image was created for each high-resolution heatmap and registered to their respective blockface images using the registration maps pre-computed in the *low-resolution histology pre-processing* module (Figure 1.4h). We stacked all registered heatmaps together to create a 3d image volume. In the *MRI pre-processing* stage, MRI datasets went through a standard pre-processing pipeline, where they are corrected for field inhomogeneity, had their background and skull removed and are automatically registered to their respective blockface volumes. The final step of the pipeline, *heatmap to MRI 3d registration*, is responsible for having the heatmaps on MRI space. In other to do so we just overlaid our registered heatmaps on the registered MRI volumes, what guaranteed that we could perform point-to-point correlations between heatmap and MRI signal. We transported the heatmap to MRI space by inverting the 3d registration maps. The resulting datasets were visualized using Freeview for 2d visualization and Amira for 3d visualizations and reconstructions.

We have used this pipeline to successfully process 524 slides from two brains with early and a late stage Alzheimer's disease, respectively. As a result, we created 3d datasets of the tau tangle heatmap for both specimens, which can be used for pure visualization or quantitative correlations with MRI signal. Figure 3

shows examples of early and late stage heatmaps overlaid on their blockface images. Here, the hotter colors indicate higher density of tau.

Neural network is effective in locating tau inclusions

The heart of our pipeline is a CNN responsible for locating tau tangle in the pre-processed histological images. We trained our models to classify pixels inside 204x204 patches of images as either tau or background. Each image tile generated by the pipeline *tiling* step (Figure 1.4d) was split into 2550 patches with 90 pixels of overlap and classified by our CNN. Unlike most common CNNs that work by outputting a single class score, our design is based on fully connected last layer, that outputs bidimensional probability maps of the tau locations. In order to quantitatively assess the performance of our CNN, we computed the receiver operating characteristic (ROC) curves for the AT8 and AT100 markes. Moreover, we computed the ROC for both the testing and validation datasets. The AT8 model obtained the area under the curve (AUC) of 0.85 for in both datasets, while the AT100 model performed a little better on the validation dataset – 0.87 on training dataset and 0.89 on the validation dataset. Figure 4 shows the ROC graphs. Figure 5 shows an example of histology tile (left) and the probability map created by the CNN (middle) and the thresholded binary mask (right).

We set the tau segmentation threshold value to 0.7, meaning only pixel with a confidence of being tau equal or larger than that value would be classified as such. In Figure 6 we can see where this threshold – indicated by the red stars on the graphs - falls on the Precision-Recall curve, for AT8 and AT100 testing and validation datasets. This value was chosen heuristically to guarantee high precision, thus reducing the number of false positives and guaranteeing that most pixels classified as tau really belong to that class.

3d tau maps

The final product of our pipeline was four 3d tau distribution datasets, showing the distribution of tau stained for AT8 and AT100, on two entire whole human brains. Figure 8 shows examples of tau map volumetric rendering overlaid on blockface images. The figure on the right shows AT100 marker distribution on the early stage AD specimen and the figure on the left shows the same marker distribution in the late stage case. Both images were rendered in the hippocampus area, a brain region traditionally affected by AD, to show the contrast between an early and late stage case.

Discussion

Here we reported a scalable, parallelizable framework for mapping tau protein in whole human brains histological slides. Our framework was used to create 3d tau distribution maps that can easily be compared point-to-point to other neuroimaging modalities. Figure 6 shows a volumetric render of such maps. During this research we had to overcome three major challenges: (1) dealing with large, unpredictable image deformation that precludes registration; (2) performing large-scale image segmentation on several hundreds of images; and (3) dealing with the large amount of data.

Materials and Methods

Specimen Procurement and Histological Processing

Two brains from patients with early and late stage AD were procured at the morgue of the San Francisco Veteran Affairs Hospital (SF-VA) by a certified technician and severed at the level of the cervical spinal cord and removed *in toto*. Both specimens were fixed by immersion in 10% buffered paraformaldehyde for 3 weeks. The brains were stored hanging by the circle of Willis for 3 days and thereafter, were fixed with the base siting on a plastic skull base molded after the subject's computerized tomography obtained as part of the in-vivo imaging exam. After fixation, the specimens were embedded in celloidin and the blocks allowed to congeal. The blocks were sectioned using a sliding microtome (AO 880, American Optical, USA) equipped with a 14" long C-knife. The brains were sectioned in serial sets of coronal slides starting from the occipital pole, each set containing 100 μm-thick sections. During block sectioning, digital photographs were acquired directly from the blockface following each cut, to obtain an accurately aligned stack of unstained serial section photographs. The pictures were taken with a high definition DSLR camera (EOS 5D Mark II, Canon, Tokyo, Japan) mounted on a copy stand arm (Kaiser Fototechnik,

Germany) and linked to a computer. Histological sections were stored in 70% alcohol for further processing.
All 1st sections from each set were immunostained to detect tau protein phosphorylated at epitopes pSer202+Thr205 (AT8, Thermo). All 2nd sections from even numbered sets were immunostained to detect tau protein phosphorylated at epitopes pThr212+Ser214 (AT100, Thermo). Finally, all 2nd sections from odd numbered set were immunostained to detect tau protein at alternative conformation (MC1, Peter Davies). Immunohistochemistry reactions were done in batches of 50 to ensure homogeneity. Each batch contained a positive and a negative control for comparison. The controls were serial sections from a single subject not belonging to the study for quality control purposes
For the quality verification process, LTG visually reviewed the positive control slide of each batch and compared the staining process to other tissue stained with the same antibody to assess the adequacy of the staining process. Staining was deemed unacceptable if no staining was present, very weak staining was observed as compared to another stained positive control slides, and/or very strong background, similar to the level of staining, was observed. Batches whose positive control was deemed unacceptable were excluded and the staining process was repeated on a second set of contiguous tissue sections, which in turn went through the same quality control process.

Whole Slide Imaging

For the described project, we developed our own cost-effective whole slide scanner (Figure 7). The hardware is comprised of a high-precision, 6” travel range, industrial XY stage (Griffin Motion), an Olympus manual focusing box, color CCD camera (Qimaging Micropublisher 6) and 5.5X machine vision objective (Navitar Zoom 6000) mounted directly on the camera. A lightbox with diffuser, mounted on top of the XY stage, is used for illumination. Slides are loaded directly to a 3d printed slide mount, on top of the lightbox. The scanner is controlled by a software developed in-house using Macro Manager 2.0.
Stitching: tiles are stitched together to form a high-resolution histological image using TeraStitcher, which is capable of working with several Gigabytes of data while maintaining a small memory footprint. During the stitching process a 10% resolution version of the image is also created and is used during the histology pre-processing and registration steps and also for visual inspection. This setup yielded a 1.22um pixel resolution.

Dataset Creation

In order to create our training, testing and validation datasets, we drew 1024x1024 pixel patches from randomly selected gray matter locations throughout the entire full-resolution brain image dataset. A set of 100 patches was created for each marker (*at100* and *at8*), from each brain respectively, totaling 4 datasets. The patch extraction routine was written in Python and completely automated, running on UCSFs’ Wynton cluster in an embarrassingly parallel way.
Each patch was manually masked for background and tau with help of Fiji’s Trainable Weka Segmentation plugin. Here, the user manually selected sample pixels belonging to *tau* and background classes that were, in turn, used to compute several features such as Gaussian filters, Hessian, membrane projections, mean, maximum, anisotropic diffusion, Lipschitz, Gabor, Laplacian, entropy, Sobel, difference of Gaussians, variance, minimum, median, bilateral filter, Kuwahara, derivatives, structure, and neighbor values. A linear SVM classifier (LibLinear) was then used to generate an initial tau segmentation. The user would retrain and refine the initial segmentation until they obtained satisfactory results. Masks where manually fine-tuned using an image editor (Gimp). All final masks went thought quality control by a highly experienced pathologist.
Finally, Patches for each maker were combined on bigger datasets, totaling 2 datasets of 200 patches each and were randomly split in 80% of patches for training, 10% for testing and the remaining for validation.

Histology Pipeline

Pre-processing blockface images

Blockface images have their background segmented using a semi-automated graph-based algorithm. Briefly, the user selects brain and background sample pixels using a graphical user interface (GUI). Images are then converted to LAB color space and the algorithm computes mean color difference maps (ΔE). ΔE is defined as the distance in LAB space:

$$\Delta E = \sqrt{L_{diff}^2 + A_{diff}^2 + B_{diff}^2}$$

With L_{diff}, A_{diff}, B_{diff} being the difference values computed as:

$$L_{diff} = L_i - \mu(L_r)$$
$$A_{diff} = A_i - \mu(A_r)$$
$$B_{diff} = B_i - \mu(B_r)$$

Where L_i, A_i and B_i are image LAB channels, L_r, A_r, B_r are LAB channels of reference pixels selected by the user, and μ(.) is the mean. Pixels in ΔE, whose color is similar to the reference values, appear dark in (smaller distance) while cell pixels are brighter (larger distance). We compute brain and background ΔE maps using the manually selected pixels as reference values and perform a histogram threshold using the Otsu's method to obtain binary masks. We, in turn, combine both masks to obtain the brain segmentation.

It is common that several undesired objects linger after the initial segmentation. It is usually caused by reflections from liquid on top of the celloidin block. The segmentation is further refined using a graph-based method to remove the undesired objects. In this method, image objects and their relationship are modelled as a weighted graph, where connected structures are considered the vertices. Edge weights are computed using a similarity function computed from color and distance values. The graph is partitioned using NCuts, leaving just the brain area.

Commonly, the camera or brain have to be repositioned several times during sectioning to adjust for changes in block size, causing the blockface images to be misaligned in relation to each other. We use semi-automatic registration to correct this artifact. Having the middle slice as the reference image, we use Matlabs' registration GUI to select landmarks for computing affine registrations. Finally, the aligned blockface images are stacked together to form the blockface 3d volume using ITK. This 3d volume is later used as an intermediate space for creating the 3d tau-protein maps.

Low-res histology background segmentation

The 10% resolution histological image is converted to LAB color space. In that space, background pixels are consistently darker than brain pixels and segmentation is performed through histogram thresholding using the triangle algorithm. The resulting binary masks, here denominated brain masks, are used to erase all background pixels. Moreover, brain masks are combined with white matter mask to create gray matter masks that guide the entire segmentation process and are also used during patch extraction for generating our training and validation datasets.

2d registration to blockface image

After background segmentation, the 10% resolution histological images are aligned to their respective blockface images using a combination of manual and automatic registration. Due to presence of an excessive number of artifacts caused by histological processing, such as tearing, shrinking and shearing, we decided for a manual initialization of the registration using MIPAV spline-based registration. Here, the user manually selects landmarks on both the histology and blockface images. MIPAV then generates a warped image and a registration warp file. After the initial registration, the image goes through a diffeomorphic registration using the 2d SyN algorithm, which is based on the large deformation diffeomorphic deformation model metric mapping (LDDMM) method. Both the registered images and registration mappings are saved for use later in the pipeline.

Image and Mask Tiling

Here, each full-resolution histological image is first tiled to reduce memory footprint during image segmentation, with tile size corresponding to approximately to 5mm^2 of tissue. Tile coordinates and dimensions are saved as XML metadata files. The histological images' respective 10% resolution gray matter masks are then rescaled to match their full-resolution dimension and tiles following the same procedure used for histology. Finally, histological tiles are masked using their respective gray matter tiles, leaving only the regions of interest on the image. Tile that are left empty or having less than 5% of tissue pixels are ignored during segmentation. This way we reduce the overall computational time and guarantee we are only processing relevant information. Image and mask tiling routines were developed in Python and ran on UCSFs' Wynton cluster in an embarrassingly parallel way, having one pipeline instance for each histological image.

Deep-learning based segmentation

A convolutional neural network is the core of our segmentation pipeline. We designed the SlideNet, a UNet based neural network capable of working with color information and outputting tau presence confidence maps that are later thresholded to create binary maps.

Model development and training

Our input layer has 204x204 pixels in RGB format, what is equivalent to a 1mm of tissue using our WSI scanner resolution. The image is pushed through three contractions blocks, the bottleneck, and upsampled by three expansion blocks. Each contraction block is composed of two convolution layers followed by a max pooling layer. Each expansion block is composed of an upsampling layer followed by two convolutional layers. While the first and second expansion blocks work with 2x upsampling, the third block works with a 3x upsampling layer. All contraction blocks' convolutional layers use 3x3 kernels with stride 1, while the bottleneck and convolutional layers at the last expansion block use 1x1 kernels with stride 1. The second convolutional neural network of each contraction block is concatenated with the upsampled data. The las convolutional layer outputs a 200x200x2 tensor that is reshaped to 20000x2 dimension. The last network layer work with the softmax activation.

Training is performed using standard backpropagation, using cross entropy as the loss function and the Adam algorithm for optimization. The learning rate is estimated using the cyclical learning rate method. We trained the network using minibatches of 32 images during 100 epochs, or until the loss curve plateaued. We also used massive data augmentation, performing real-time random rotations, shear, horizontal and vertical flips. SlideNet code was developed in Keras and ran on a NVIDIA Titan X GPU with 12Gb of RAM.

SlideNet outputs confidence maps of the existence of tau, which are thresholded to generate binary masks. Threshold value was set to 0.7 for both AT100 and AT8 datasets and pixel with confidence higher than this value were considered tau.

Heatmap computation

The binary tiles are transferred back to our cluster, where the heatmaps are computed. On each tile, we compute the mean amount of tau, indicated by the mean number of pixels belonging to foreground, inside a 1 μm^2 of tissue, roughly an 8x8 pixels block. The heatmaps are generated as tiles having the same dimension of binary tiles where each 1 μm^2 block is filed out with the mean number of pixels belonging to tau. Tiles are stitched together to create a heatmap having the same resolution as the original histological image and is latter resized to 10% of its resolution.

Heatmap normalization

Heatmaps are normalized to a reference slide. Our normalization procedure is inspired by grayscale histogram matching algorithms. Our method works by adjusting the histogram of the target images to that of a reference image. Since our images are continuous, we begin by binning them in 1000 bins and computing their normalized histograms. We then compute the cumulative distribution function (CDF) for both histograms. For each non-background pixel in the target image, we use the CDF to map its value to a bin and get its edge values. We then find the closest match to the target pixel CDF value in the reference image CDF and use the later to retrieve its respective bin edges. We finally obtain the normalized value by computing a linear mapping of the target pixel value from [c,d] to [a,c]. Our normalization step was developed in Python and run on Wynton in an embarrassingly parallel task.

Heatmap to blockface alignment and stacking

The 2d registration maps computed during the 2d registration to blockface image step are applied to the 10% resolution normalized heatmaps, yielding heatmap registered to their respective blockface images. These images are then stacked together to for a 3d volume.

MRI pipeline

Field inhomogeneity correction

Since field intensity inhomogeneity may reduce the overall processing quality, we begin our processing with a correction step for this artifact, using the previously validated N3 algorithm.

Brain segmentation

This step aims to eliminate all background noise and unnecessary information (such as bones and meninges) from the images that could cause registration errors and slow down the computational processing. We perform the segmentation by using the FSL BET tool.

Spatial Resampling

Histological images have higher resolution than their MRI counterparts. While digitized histology voxels have sub-millimetric volume, a standard clinical MRI acquisition has a voxel size of around 1x1x1 mm. Direct registration of these images will cause the histology to be resampled to a lower resolution space, introducing loss of contrast and anatomical information of interest. We instead upsample the MRI volume to a higher resolution space (0.33x0.33x0.33 mm voxel size) by employing the cubic splines interpolation. We found this resolution to be computationally tractable, while still allowing visualization of fine details in histological images, such as deep brain structures – i. e. hippocampi, substantia nigra, and caudate nucleus. Figure 3f shows the same slices before (first row) and after (second row) skull stripping.

Histology to MRI 3D registration

Three-dimensional histology to MRI registration is performed using the 3D SyN algorithm. SyN is based on the large deformation diffeomorphic deformation model metric mapping (LDDMM) method whose mathematical properties are especially appealing for our problem. Diffeomorphic maps are smooth and invertible functions guaranteeing that no folds or vanishing tissue will occur during the registration process. These models also enforce a 1-to-1 mapping between the movable and reference voxels and are suitable to handle large deformations. SyN is a mature method that has been reported to outperform several popular registration methods. Here, SyN is used with Mattes mutual information for measuring similarity, given that it is the most robust option for handling multi-modality registration problems. All 3D registration maps computed in this step are stored for future use. Figure 3h is an example of 3D histology to MRI registration using the described method. The first row shows sagittal, axial, and coronal checkerboard representations of a histology slice, overlaid on its respective MRI. The right-hand side shows a 3D rendering of one registered volume overlaid on its MRI.

3d Reconstruction and Visualization

The 3d registration maps generated during the **Histology to MRI 3D registration** are inverted and used to warp the MRI to blockface space, allowing direct comparison between MRI signal and tau density. Freeview is used for visualization of 2d slices. Amira (ThermoFisher Scientific) is used for 3d reconstruction and visualization.

Declarations

Acknowledgements

We would like to thank the support of NVIDIA Corporation with the donation of a Titan V GPU.

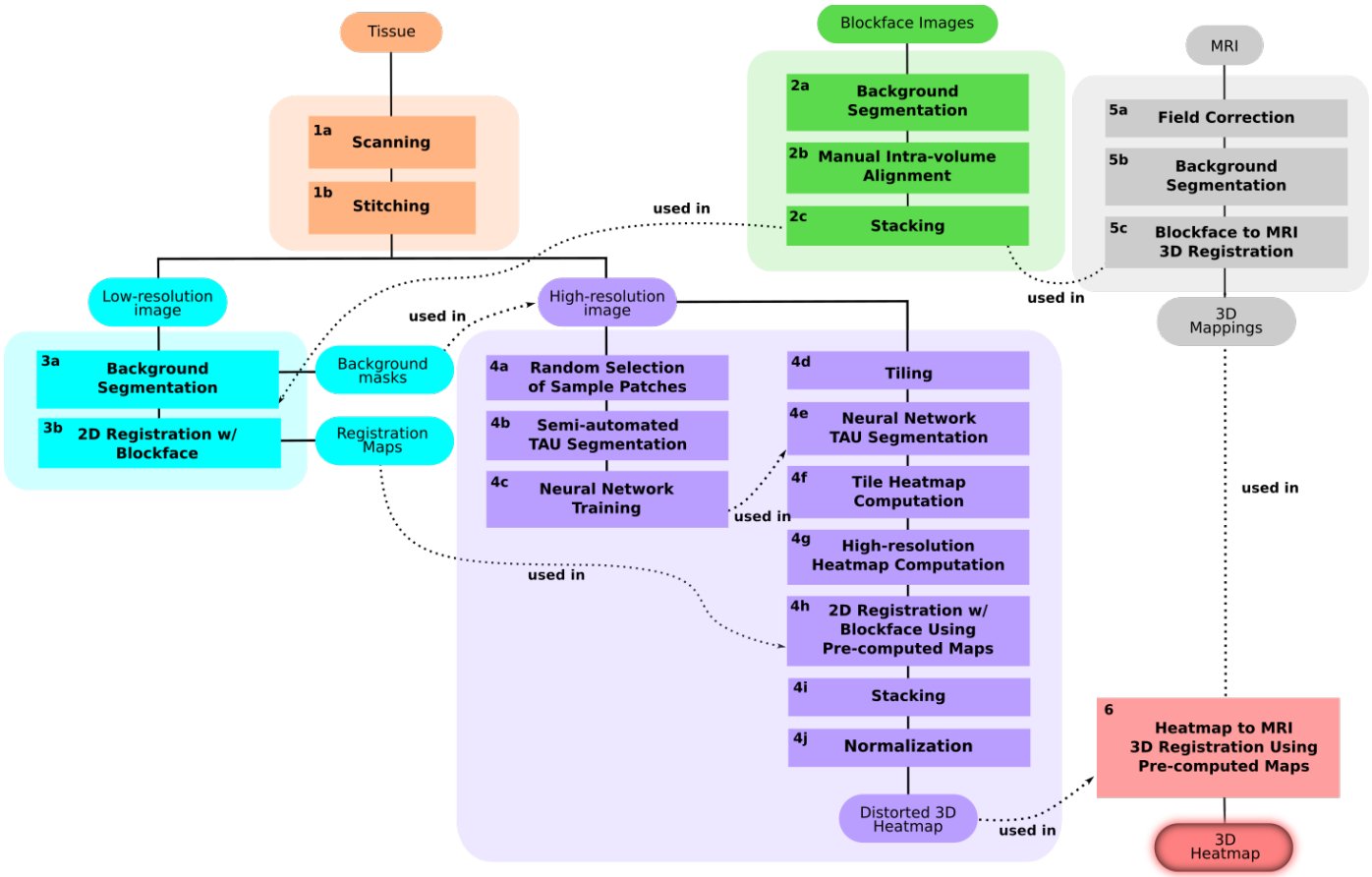

Figure 1: Tau tangle mapping pipeline. 1. Imaging module; 2. Blockface pre-processing module; 3. Low-resolution histology pre-processing module; 4. High-resolution histology segmentation module; 5. MRI pre-processing module; 6. 3d heatmap to MRI registration.

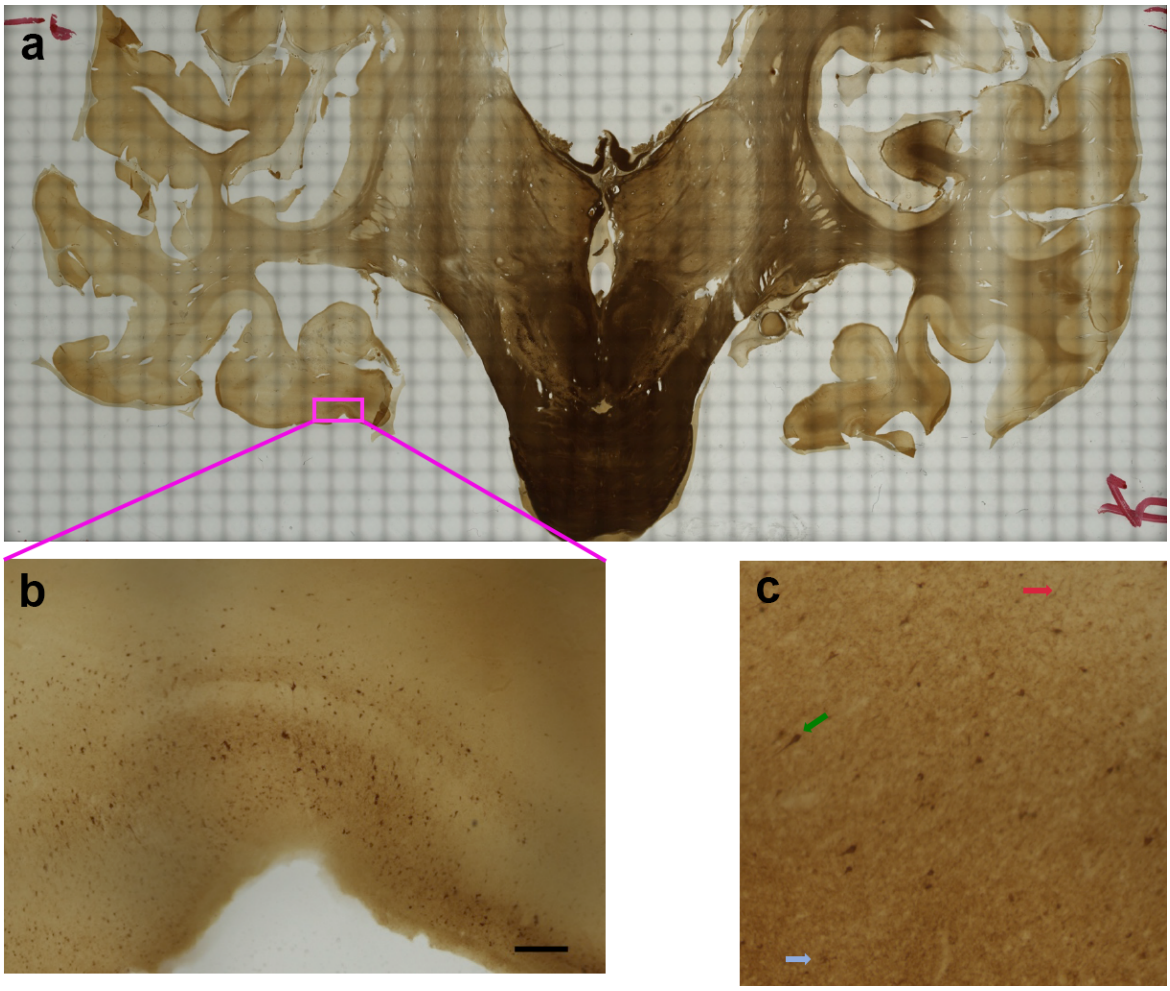

Figure 2: a) example of stitched image; b) 100% zoom of a hippocampus area (scalebar is 0.3mm); c) example of tau inclusions our system is capable of detecting. Green arrow is shows an NFT, red arrow shows a thread and blue arrow show as plaque.

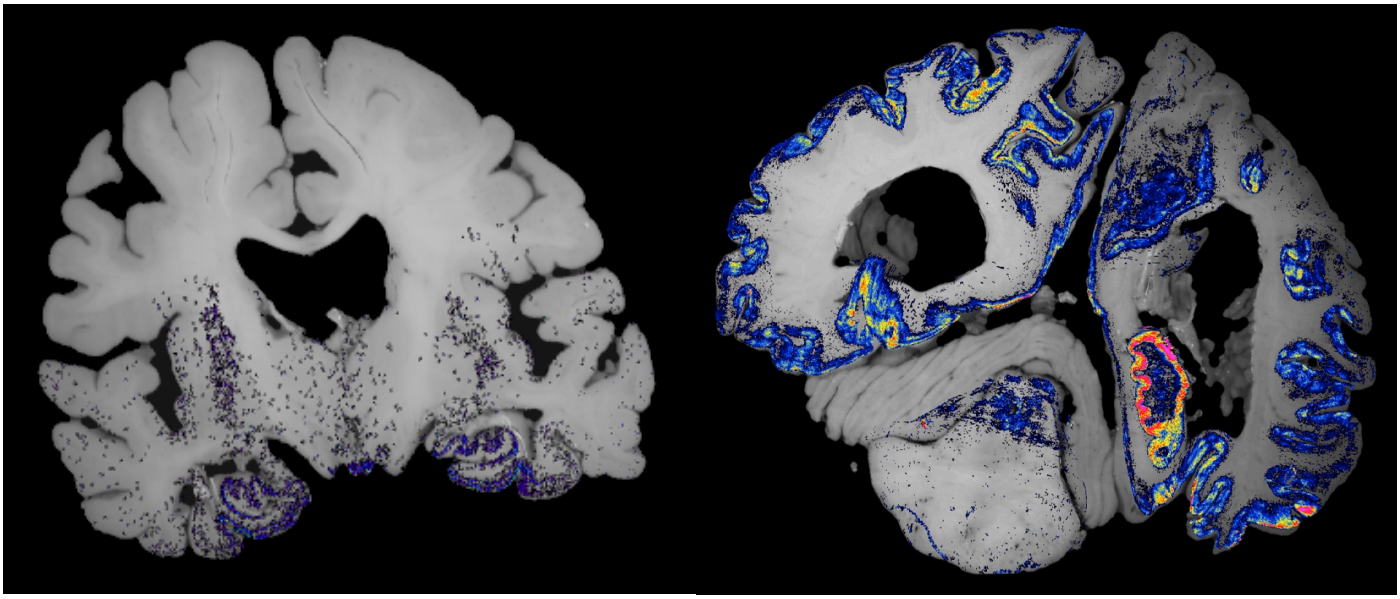

Figure 3: Examples of a heatmap from the early (left) and late (right) stage specimens. Here, warmer colors indicate higher density of tau tangles.

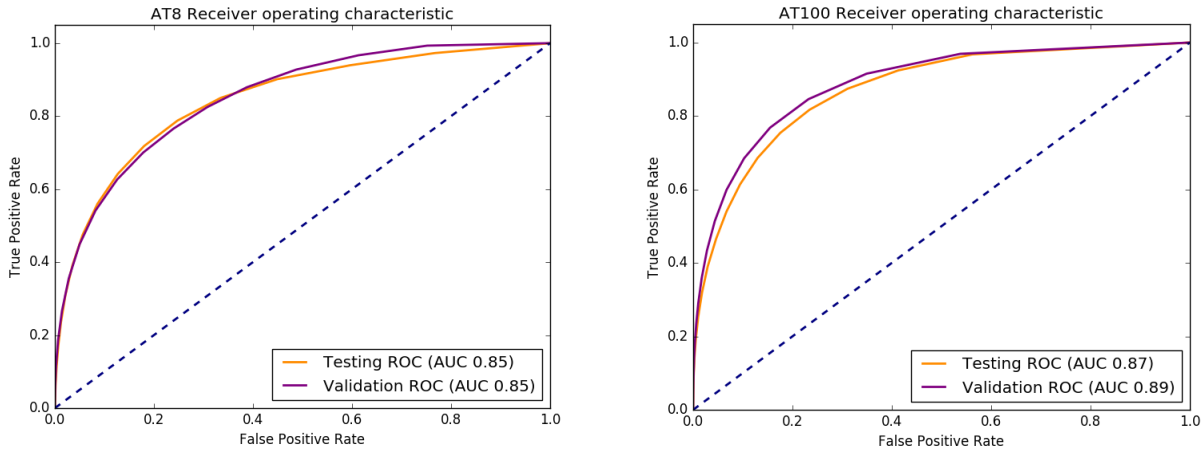

Figure 4: ROC curves

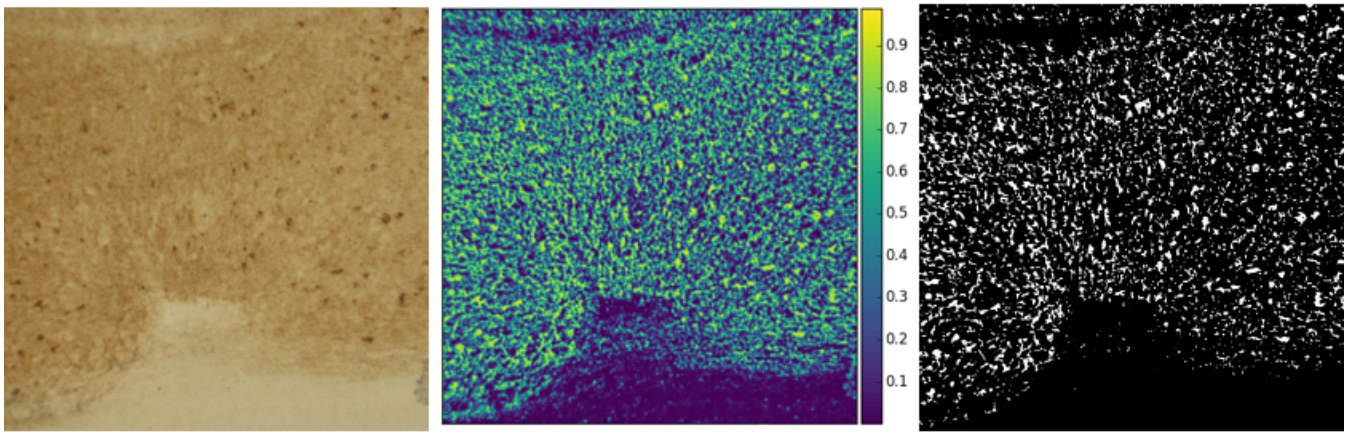

Figure 5: AT8 stained image patch (left) and its respective probability map (middle) and binary segmentation after thresholding at 0.7 (right)

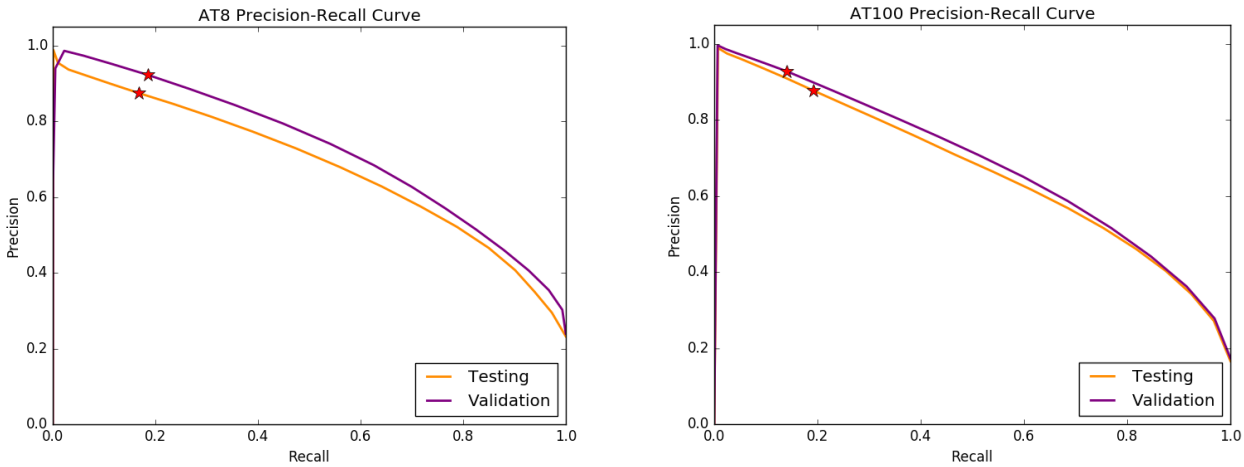

Figure 6: Precision-Recall curves for the AT8 and AT100 models. The red star indicates where is the 0.7 probability, which is used for thresholding the probability maps

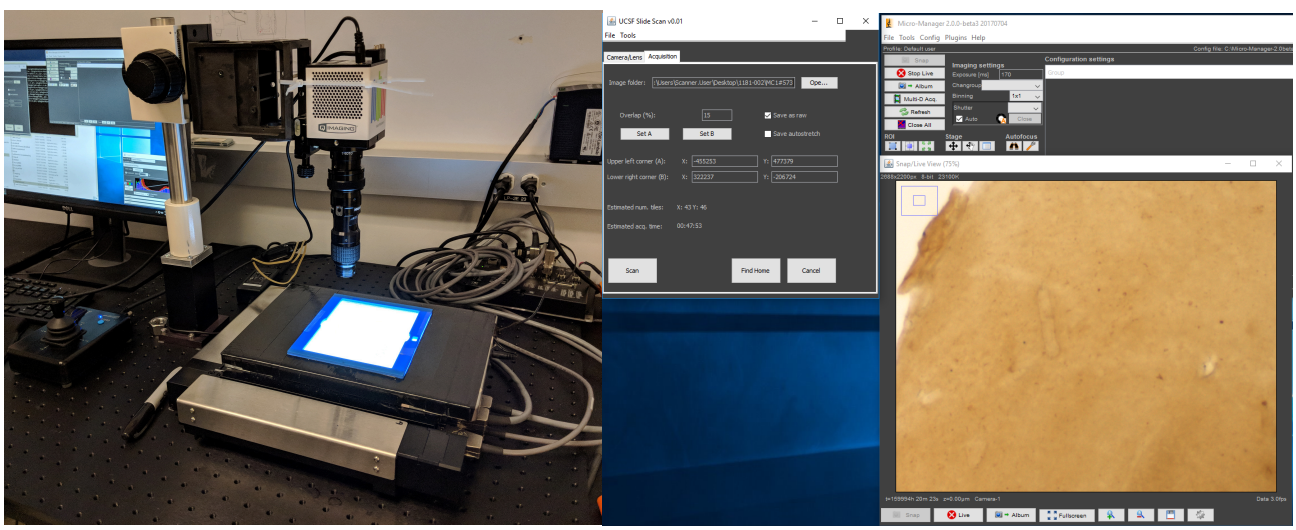

Figure 7: Left: our customized whole slide scanner. Right: User interface of the controller software developed using Micro Manager 2.0

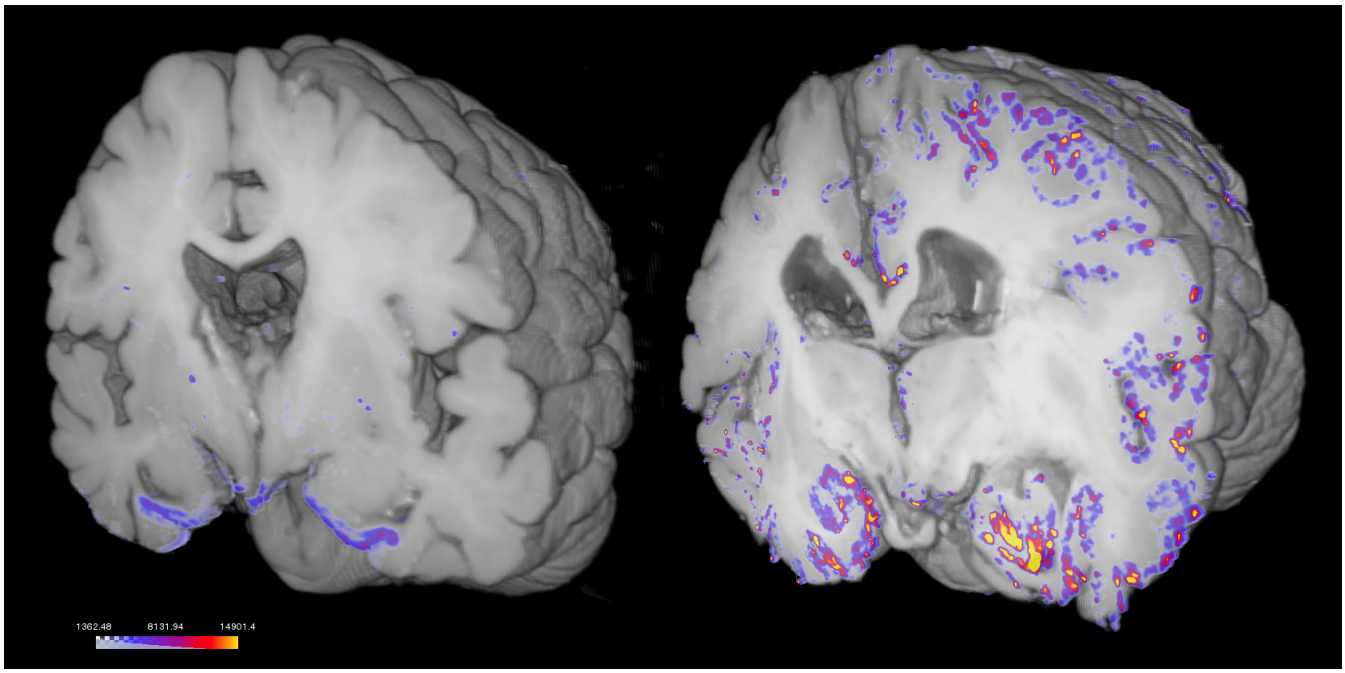

Figure 8: Volumetric reconstruction of the early (left) and late stage (right) AT100 tau heatmaps around the hippocampus area, overlaid on their respective blockface volumes

References

1. Montine, T.J., et al., *National Institute on Aging-Alzheimer's Association guidelines for the neuropathologic assessment of Alzheimer's disease: a practical approach.* Acta neuropathologica, 2012. **123**(1): p. 1-11.
2. Jack, C.R., Jr., *Alzheimer disease: new concepts on its neurobiology and the clinical role imaging will play.* Radiology, 2012. **263**(2): p. 344-61.
3. Grinberg, L.T. and H. Heinsen, *Light at the beginning of the tunnel? Investigating early mechanistic changes in Alzheimer's disease.* Brain: A Journal of Neurology, 2017. **140**(11): p. 2770-2773.
4. Simic, G., et al., *Does Alzheimer's disease begin in the brainstem?* Neuropathology and Applied Neurobiology, 2009. **35**(6): p. 532-554.
5. Theofilas, P., et al., *Turning on the Light Within: Subcortical Nuclei of the Isodentritic Core and their Role in Alzheimer's Disease Pathogenesis.* Journal of Alzheimer's disease: JAD, 2015. **46**(1): p. 17-34.
6. Theofilas, P., et al., *Locus coeruleus volume and cell population changes during Alzheimer's disease progression: A stereological study in human postmortem brains with potential implication for early-stage biomarker discovery.* Alzheimer's & Dementia: The Journal of the Alzheimer's Association, 2017. **13**(3): p. 236-246.
7. Theofilas, P., et al., *Probing the correlation of neuronal loss, neurofibrillary tangles, and cell death markers across the Alzheimer's disease Braak stages: a quantitative study in humans.* Neurobiology of Aging, 2018. **61**: p. 1-12.

8. Ehrenberg, A.J., et al., *Quantifying the accretion of hyperphosphorylated tau in the locus coeruleus and dorsal raphe nucleus: the pathological building blocks of early Alzheimer's disease.* Neuropathology and Applied Neurobiology, 2017. **43**(5): p. 393-408.
9. Bartzokis, G., *Alzheimer's disease as homeostatic responses to age-related myelin breakdown.* Neurobiology of aging, 2011. **32**(8): p. 1341-1371.
10. Benitez, A., et al., *White matter tract integrity metrics reflect the vulnerability of late-myelinating tracts in Alzheimer's disease.* Neuroimage Clin, 2014. **4**: p. 64-71.
11. Sachdev, P.S., et al., *Is Alzheimer's a disease of the white matter?* Curr Opin Psychiatry, 2013. **26**(3): p. 244-51.
12. Braak, H., et al., *Stages of the pathologic process in Alzheimer disease: age categories from 1 to 100 years.* Journal of Neuropathology and Experimental Neurology, 2011. **70**(11): p. 960-969.
13. *2018 Alzheimer's disease facts and figures.* Alzheimer's & Dementia: The Journal of the Alzheimer's Association, 2018. **14**(3): p. 367-429.
14. Duyckaerts, C., B. Delatour, and M.-C. Potier, *Classification and basic pathology of Alzheimer disease.* Acta Neuropathologica, 2009. **118**(1): p. 5-36.
15. Cullen, K.M. and G.M. Halliday, *Neurofibrillary degeneration and cell loss in the nucleus basalis in comparison to cortical Alzheimer pathology.* Neurobiology of Aging, 1998. **19**(4): p. 297-306.
16. Gomez-Isla, T., et al., *Neuronal loss correlates with but exceeds neurofibrillary tangles in Alzheimer's disease.* Ann Neurol, 1997. **41**(1): p. 17-24.
17. Seeley, W.W., et al., *Neurodegenerative diseases target large-scale human brain networks.* Neuron, 2009. **62**(1): p. 42-52.
18. Okamura, N., et al., *The development and validation of tau PET tracers: current status and future directions.* Clinical and translational imaging, 2018. **6**(4): p. 305-316.
19. Saint-Aubert, L., et al., *Tau PET imaging: present and future directions.* Molecular Neurodegeneration, 2017. **12**(1): p. 19.